DNA demethylation fine-tunes IL-2 production during thymic regulatory T cell differentiation

Athmane Teghanemt[1,2] , Kara Misel-Wuchter[2,3] , Jace Heath[2,4] , Andrew Thurman[1], Priyanjali Pulipati[1,2] , Garima Dixit[1,2] , Ramasatya Geesala[1,2] , David K Meyerholz[5] , Thorsten Maretzky[1,2] , Alejandro Pezzulo[1] & Priya D Issuree[1,2,3,4,*]

Abstract

Regulatory T (T reg) cells developing in the thymus are essential to maintain tolerance and prevent fatal autoimmunity in mice and humans. Expression of the T reg lineage-defining transcription factor FoxP3 is critically dependent upon T cell receptor (TCR) and interleukin-2 (IL-2) signaling. Here, we report that ten-eleven translocation (Tet) enzymes, which are DNA demethylases, are required early during double-positive (DP) thymic T cell differentiation and prior to the upregulation of FoxP3 in CD4 single-positive (SP) thymocytes, to promote Treg differentiation. We show that Tet3 selectively controls the development of $CD25^-$ $FoxP3^{lo}$ CD4SP Treg cell precursors in the thymus and is critical for TCR-dependent IL-2 production, which drive chromatin remodeling at the FoxP3 locus as well as other Treg-effector gene loci in an autocrine/paracrine manner. Together, our results demonstrate a novel role for DNA demethylation in regulating the TCR response and promoting Treg cell differentiation. These findings highlight a novel epigenetic pathway to promote the generation of endogenous Treg cells for mitigation of autoimmune responses.

Introduction

Regulatory T (Treg) cells are an essential lineage of $CD4^+$ T lymphocytes that are demarcated by expression of the X-linked transcription factor FoxP3 and which mediate the establishment and maintenance of immunological self-tolerance and homeostasis in humans and mice (Sakaguchi *et al*, 2008; Josefowicz *et al*, 2012).

Deficits in the number of circulating Treg cells and/or compromised Treg cell function are closely associated with multiple autoimmune disorders including multiple sclerosis and type 1 diabetes (Miyara *et al*, 2011). FoxP3 deficiency or mutations in the *Foxp3* gene also lead to severe autoimmune diseases and immunopathology in mice and humans, exemplifying the importance of FoxP3 in maintaining the Treg cell functional program (Sakaguchi *et al*, 2020). The transcriptional maintenance of *Foxp3* expression is heavily dependent on DNA demethylation facilitated by ten-eleven translocation (Tet) enzymes which are Fe (II) and 2-oxoglutarate-dependent dioxygenases that mediate the iterative oxidation of the methyl group of 5-methylcytosine (5mC) to various intermediates (Wu & Zhang, 2017).

Tet enzymes are a family of three members Tet1, Tet2, and Tet3, all of which are expressed in T cells (Lio & Rao, 2019). It was previously shown that combined deletion of Tet2 and Tet3 early during T cell development, in double-positive (DP) thymocytes, results in a massive expansion of invariant natural killer T (iNKT) cells, and a significant loss of Treg proportions and function in the periphery due to a loss of FoxP3 expression in activated Tregs (Yue *et al*, 2016; Tsagaratou *et al*, 2017). Stable *Foxp3* gene expression is closely linked to the methylation status of a "conserved non-coding sequence" CNS2 within the *Foxp3* locus (Floess *et al*, 2007). This regulatory element is demethylated in a Tet2/3-dependent manner and has been shown to be essential for maintaining stable expression in effector Treg cells (Floess *et al*, 2007; Zheng *et al*, 2010; Toker *et al*, 2013). Consequently, Tet2/3-deficient mice have impaired Treg cell functions, exhibit autoimmune-like pathologies, and succumb to early death (Yue *et al*, 2016). Interestingly, combined deletion of Tet2 and Tet3 specifically in Treg cells also results in a replication-dependent loss of *Foxp3* gene expression and other Treg signature genes such as *Il2ra*, leading to inflammatory disease and early death in mice (Yue *et al*, 2019). Together these findings strongly demonstrate that Tet2 and Tet3 are critical for the maintenance of stable transcriptional programs and function in Treg cells.

1 Department of Internal Medicine, Roy J. and Lucille A. Carver College of Medicine, University of Iowa, Iowa City, IA, USA
2 Inflammation Program, Roy J. and Lucille A. Carver College of Medicine, University of Iowa, Iowa City, IA, USA
3 Molecular Medicine Graduate Program, Iowa City, IA, USA
4 Immunology Graduate Program, Iowa City, IA, USA
5 Department of Pathology, University of Iowa, Iowa City, IA, USA
*Corresponding author. Tel: +1 319 335 3668; E-mail: priya-issuree@uiowa.edu

It is currently unclear whether DNA demethylation controls other aspects of Treg biology independent of their role in the maintenance of transcriptional programs in Treg cells. Treg cells are distinctively programmed via epigenetic mechanisms during their differentiation from CD4^{+} precursors in the thymus. A significantly large portion of Treg-specific enhancers are poised for activity in the precursor stages, prior to FoxP3 expression, via the concerted action of DNA binding proteins such as Satb1 (special AT-rich sequence-binding protein 1) and Mll4 (myeloid/lymphoid or mixed-lineage leukemia 4). Consequently, such enhancers exhibit unique chromatin and histone signatures prior to differentiation (Kitagawa *et al*, 2017; Placek *et al*, 2017). Using the *Cd4* gene as a model locus to understand the role of DNA methylation during CD4 T cell development, we previously showed that Tet enzymes initiate DNA demethylation immediately following positive selection in the thymus and shape the enhancer landscape in conventional CD4^{+} T cells (Sellars *et al*, 2015; Issuree *et al*, 2018; Teghanemt *et al*, 2022). Genome-wide assessment of the DNA methylation landscape in developing thymocytes has also supported this finding (Tsagaratou *et al*, 2014), and alterations in DNA methylation patterns can be detected in early stages of thymic Treg cell development prior to the expression of FoxP3 (Polansky *et al*, 2008; Ohkura *et al*, 2012). However, the impact of these early epigenetic changes on Treg cell lineage differentiation is not clear.

In this present study, we show that Tet3 is specifically required at the double-positive (DP) stage of thymic T cell development to calibrate the ability of developing CD4^{+} T cells to produce IL-2 in a TCR-dependent manner and differentiate into Treg cells, highlighting for the first time, to our knowledge, that DNA demethylation modulates Treg development in the thymus in a TCR/IL-2-dependent manner. We show that this calibration is required in precommitted Treg cells, such that loss of Tet1/3 in FoxP3-expressing cells does not impede their development into Treg cells or their maintenance in the periphery. We show that Tet3 selectively regulate the development of CD25^{−}FoxP3^{lo} precursor Treg cells from CD4 T cells and control Treg cell differentiation by modulating T cell receptor (TCR) signaling and IL-2 production. Importantly, we show that Tet1 and Tet3 are not required for the maintenance of Treg lineage programs highlighting distinct and nonredundant roles of Tet enzyme family members and a critical role for Tet2 in that regard. We demonstrate that early developmental programming in CD4^{+} T cells is also critical for *in vitro* Treg cell differentiation by calibrating the cell-autonomous TCR and IL-2 responses, which are critical to drive FoxP3 expression as well as shape the chromatin landscape of differentiating Treg cells in a STat5-dependent manner. Taken together, our data report for the first time that Tet enzymes are required for the differentiation of Treg cells from CD4^{+} T cells and identify a critical window during which modulation of Tet1/3 activity may be a clinically relevant opportunity to increase the generation of endogenously derived Treg cells.

Results and Discussion

Loss of Tet1 and Tet3 during thymic development leads to a decrease in regulatory T cells

During the process of investigating the unique contributions of enzymes in T cell development, we had initially observed that similar to *Cd4*[CreTg] *Tet2/3*[fl/fl] mice, *Rorc(t)*[CreTg] *Tet1/2/3*[fl/fl] mice (referred to as Tet1/2/3[cTKO] mice), in which Tet alleles are deleted at the double-positive stage during thymic T cell development (Eberl & Littman, 2004), developed severe lymphoproliferative disease, with a disease onset of 3 weeks and early death between the ages of 10–20 weeks (Fig 1A). Tet1/2/3[cTKO] mice exhibited a gross loss of

---

Figure 1. Loss of Tet1 and Tet3 during thymic development leads to a decrease in regulatory T cells.

A Survival curves for control (*n* = 23 biological replicates), *Rorc(t)*[CreTg] *Tet1/3*[fl/fl] (*n* = 20 biological replicates), *Rorc(t)*[CreTg] *Tet1/2/3*[fl/fl] mice (*n* = 10 biological replicates).

B Representative flow cytometry plot of CD62L and CD44 expression on conventional CD4^{+} T cells in the spleen of control and *Rorc(t)*[CreTg] *Tet1/2/3*[fl/fl] mice, pregated on Live CD4^{+}TCRβ^{+} T cells.

C Representative pictures of the spleen, LN, and mLN isolated from 3-week-old control, *Rorc(t)*[CreTg] *Tet1/2/3*[fl/fl] and *Rorc(t)*[CreTg] *Tet1/3*[fl/fl] mice. Adenopathy in the mLN was already visible in 3-week-old *Rorc(t)*[CreTg] *Tet1/2/3*[fl/fl] mice.

D Representative flow cytometry plot of CD62L and CD44 expression on conventional CD4^{+} T cells in the spleen, pregated on Live CD4^{+}TCRβ^{+} T cells and quantification of the frequency of CD62L^{hi}CD44^{lo} among CD4 T cells in the spleen of control *Tet1/3*[fl/fl] (*n* = 7 biological replicates) and *Rorc(t)*[CreTg] *Tet1/3*[fl/fl] mice (*n* = 9 biological replicates). Data are mean ± SEM, unpaired Mann–Whitney *t*-test.

E Representative H&E staining of the lungs (top panel) and small intestine (bottom panel) and histopathological scoring of 3-month-old control (*n* = 3 biological replicates) and *Rorc(t)*[CreTg] *Tet1/3*[fl/fl] mice (*n* = 3 biological replicates). Data are mean ± SEM, one-way ANOVA with uncorrected Fisher's LSD test. Scale bar = 263 and 53 μm, top and bottom panels, respectively.

F Frequency of FoxP3^{+} cells among CD4^{+} T cells in the thymus (*n* = 6 or 10 biological replicates), peripheral lymph nodes (*n* = 5 or 6 biological replicates), spleen (*n* = 5 or 6 biological replicates), and mesenteric lymph nodes (*n* = 4 or 8 biological replicates) pregated on live CD4^{+}TCRβ^{+} T cells and representative flow plots (bottom). Data are mean ± SEM, one-way ANOVA with uncorrected Fisher's LSD test.

G Absolute number of FoxP3^{+} Tregs from the thymus (*n* = 5 or 7 biological replicates) and spleen (*n* = 7 or 8 biological replicates) of control *Tet1/3*[fl/fl] and *Rorc(t)*[CreTg] *Tet1/3*[fl/fl] mice. Data are mean ± SEM, unpaired Mann–Whitney *t*-test.

H Quantification of CD25 MFI expression on FoxP3^{+} T cells in the spleen of control *Tet1/3*[fl/fl] (*n* = 4 biological replicates) and *Rorc(t)*[CreTg] *Tet1/3*[fl/fl] mice (*n* = 4 biological replicates). Data are mean ± SEM, unpaired Mann–Whitney *t*-test.

I Quantification of FoxP3 MFI expression on FoxP3^{+} T cells in the spleen of control *Tet1/3*[fl/fl] (*n* = 6 biological replicates) and *Rorc(t)*[CreTg] *Tet1/3*[fl/fl] mice (*n* = 6 biological replicates). Data are mean ± SEM, unpaired Mann–Whitney *t*-test.

J Quantification of ICOS MFI expression on FoxP3^{+} T cells from the mesenteric lymph nodes of control *Tet1/3*[fl/fl] (*n* = 5 biological replicates) and *Rorc(t)*[CreTg] *Tet1/3*[fl/fl] (*n* = 7 biological replicates) mice. Data are mean ± SEM, unpaired Mann–Whitney *t*-test.

Data information: ns = not significant, $P > 0.05$, *$P < 0.05$, **$P < 0.01$, ***$P < 0.001$, ****$P < 0.0001$, paired male or female mice were used and no gender biases associated with genotypes were observed. (A–J) Experiments were replicated at least three times.
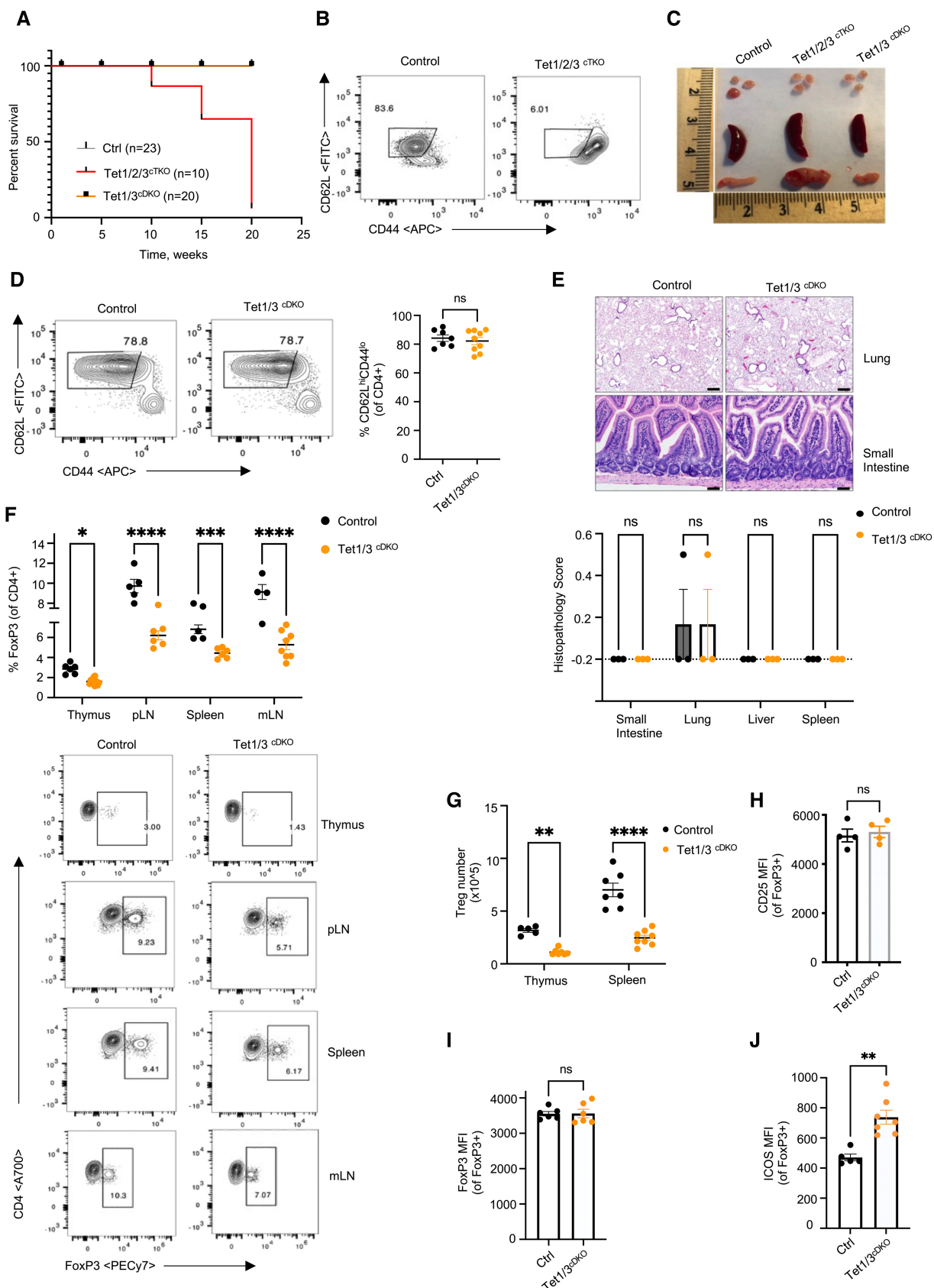
Source data are available online for this figure.

Figure 1.

naïve CD4$^+$ T cells in the periphery as assessed by CD62L and CD44 expression (Fig 1B) and lymphomegaly by 3 weeks of age (Fig 1C). However, combined loss of Tet1/2 (Yang *et al*, 2015) or Tet1/3 did not result in disease or early death in > 1-year-old mice (Fig 1A). *Rorc(t)*^{CreTg} *Tet1/3*$^{fl/fl}$ mice (hereafter referred to as Tet1/3^{cDKO} mice) were healthy, had a normal quiescent T cell compartment assessed by CD62L and CD44 expression (Fig 1D), and showed no lesions in various organs compared with wild-type (WT) littermate controls (Fig 1E). Interestingly, however, we observed a significant decrease in the proportion and numbers of FoxP3$^+$ CD4$^+$ T cells in the thymus, spleen, and peripheral and mesenteric lymph nodes of Tet1/3^{cDKO} mice compared with littermate controls (Fig 1F and G). Among FoxP3$^+$ CD4$^+$ T cells, we did not observe any statistical difference in the mean fluorescence intensity (MFI) of CD25 (Fig 1H) or FoxP3 (Fig 1I) in Tet1/3^{cDKO} Treg cells compared with control cells although Tet1/3^{cDKO} Treg cells expressed higher levels of ICOS (Fig 1J). Together these data suggest that Tet1 and Tet3 regulate the Treg cell compartment in mice in a manner distinct from the combined activities of Tet2 and Tet3.

Loss of Tet1 and Tet3 does not impair stable programs in naturally occurring Treg cells

As Tet2 and Tet3 were previously shown to regulate *Foxp3* expression and maintenance of Treg cells during replication (Yue *et al*, 2016, 2019), we assessed whether maintenance of FoxP3 and Treg cells were impaired in Tet1/3-deficient mice. In marked contrast to Tet2/3^{cDKO} or Tet1/2/3^{cTKO} Treg cells, Tet1/3^{cDKO} Treg cells maintained high FoxP3 and CD25 expression upon cellular replication (Figs 2A and B, and EV1A and B) and continued to express higher levels of ICOS compared with WT Treg cells (Fig EV1C). However, congruent with our previous findings, we observed a defect in the maintenance of CD4 expression (Fig 2C) due to the impaired function of a stimulus-responsive regulatory element within the *Cd4* gene (Issuree *et al*, 2018; Teghanemt *et al*, 2022). Together, these data suggest that Tet1/3 exhibit locus-dependent activities and do not affect transcriptional stability of the *Foxp3* gene. In agreement with this, we found only modest differences at certain CpGs

examined within *Cns2* of Tet1/3^{cDKO} Treg cells (Fig 2D). These modest differences are unlikely to be required for the maintenance of FoxP3 expression as FoxP3 expression was stable at rest and upon replication.

Next, we assessed whether the suppressive function of Tet1/3^{cDKO} Treg cells was intact. In an *in vitro* suppression assay using autologous antigen-presenting cells and conventional CD4$^+$ T cells stimulated with anti-CD3, Tet1/3^{cDKO} Treg cells were as effective as WT Treg cells in suppressing the proliferation of effector CD4$^+$ T cells at various ratios tested (Figs 2E and EV1D). In a mouse model of dextran sodium sulfate (DSS) colitis, where Treg cells have been implicated in providing protection against injury (Boehm *et al*, 2012; Wang *et al*, 2015), we did not observe any significant differences in weight loss when control or Tet1/3^{cDKO} mice were challenged with an acute dose of DSS (Fig EV1E). Tet1/3^{cDKO} mice exhibited comparable shortening of the small intestine and colon as control mice, suggestive of comparable inflammation (Fig EV1F and G). To exclude a confounding role for non-Treg cells and directly assess the intrinsic function of Tregs *in vivo*, we used a mouse model of T cell transfer colitis (Mottet *et al*, 2003). Following adoptive transfer into *Rag*$^{-/-}$ recipients, Tet1/3^{cDKO} Treg cells were equally efficient as control Tregs in suppressing the loss of weight caused by exuberant inflammation of inflammatory Type 1 helper (Th1) or Type 17 helper (Th17) effector cells (Lee *et al*, 2009; Harbour *et al*, 2015; Fig 2F). This was also true when a higher ratio of Teff:Treg T cells was transferred (Fig EV1H). The proportions of Tbet$^+$ and Rorγt$^+$ effector T cells as well as IFNγ-producing T cells were effectively suppressed by Tet1/3^{cDKO} Treg cells (Figs 2G and EV1I) and CD25 and CTLA4 expression on Tet1/3^{cDKO} Tregs were comparable to WT Treg cells (Fig EV1J). Interestingly, mice receiving Tet1/3^{cDKO} Tregs had lower proportions of Rorγt$^+$ effector T cells (Fig 2G) and a lower inflammation score by H&E-guided histopathology of the colons (Fig EV1K and L), suggesting that Tet1/3^{cDKO} Tregs may be endowed with superior suppressive function *in vivo*. As effector molecules produced by activated Tregs cells *in vitro*, such as IL-10 and Granzyme B were comparable between control and Tet1/3^{cDKO} Treg cells (Fig EV1M), this suggests that the increased suppression is plausibly due to higher ICOS expression,

---

Figure 2. Loss of Tet1 and Tet3 does not impair stable programs in naturally occurring Tregs.

A Representative flow plots, histogram and quantification of FoxP3 MFI expression in cell proliferation dye-labeled Treg cells FACS sorted from *Tet1/3*$^{fl/fl}$;Foxp3^{GFP} ($n = 3$ biological replicates) and *Rorc(t)*^{CreTg} *Tet1/3*$^{fl/fl}$;Foxp3^{GFP} ($n = 3$ biological replicates) male mice. Cells were activated *in vitro* for 72 h with anti-CD3/CD28 in the presence of 200 U/ml hIL-2. Data are mean $\pm$ SEM, unpaired *t*-test. Experiment was replicated three times.

B CD25 MFI expression in Treg cells activated as in (A). Data are mean $\pm$ SEM, unpaired *t*-test.

C Representative flow plots, histogram and quantification of CD4 gMFI expression in Treg cells activated as in (A). Data are mean $\pm$ SEM, unpaired *t*-test.

D DNA methylation assessment by amplicon-based bisulfite sequencing of 15 CpG sites present in CNS2 within the FoxP3 locus of eGFP$^+$ Treg cells isolated from *Tet1/3*$^{fl/fl}$;Foxp3^{GFP} and *Rorc(t)*^{CreTg} *Tet1/3*$^{fl/fl}$;Foxp3^{GFP} male mice. Experiment was replicated two times.

E Quantification of the percent of divided conventional CD4$^+$ T cells ($n = 3$) at 72 h in an *in vitro* suppression assay with Tregs isolated from *Tet1/3*$^{fl/fl}$ and *Rorc(t)*^{CreTg} *Tet1/3*$^{fl/fl}$ littermates. Gates were set on unstimulated CFSE-labeled conventional CD4$^+$ T cells. Data are mean $\pm$ SEM, one-way ANOVA. Paired male or female mice were used, and no gender biases associated with genotypes were observed. Experiment was replicated three times.

F Weight curve of female *Rag*$^{-/-}$ mice after T cell transfer colitis induced via transfer of naïve WT CD45.1 conventional CD4$^+$ T cells alone ($n = 5$ recipients) or in combination with Tregs isolated from *Tet1/3*$^{fl/fl}$ and *Rorc(t)*^{CreTg} *Tet1/3*$^{fl/fl}$ littermates ($n = 5$ recipients/group). Data are mean $\pm$ SEM, two-way ANOVA with Geisser–Greenhouse correction. Experiment was replicated two times.

G Representative flow plots and quantification of percent Tbet$^+$, Rorγt$^+$, and FoxP3$^+$ of CD45.1 CD4$^+$ effector cells isolated from the MLN of female *Rag*$^{-/-}$ mice 7-week post-T cell transfer-induced colitis. Respective cohorts were Naïve CD45.1 T cells only ($n = 5$ mice), WT CD45.1$^+$ *Tet1/3*$^{fl/fl}$ Tregs ($n = 5$ mice), and WT CD45.1$^+$*Rorc(t)*^{CreTg} *Tet1/3*$^{fl/fl}$ Tregs ($n = 4$ mice). Cells were pregated on Live CD45.1$^+$TCRβ$^+$ cells. Data are mean $\pm$ SEM, two-way ANOVA with Tukey's Multiple comparison test. Experiment was replicated two times.

Data information: ns = not significant, $P > 0.05$, *$P < 0.05$, **$P < 0.01$, ****$P < 0.0001$.
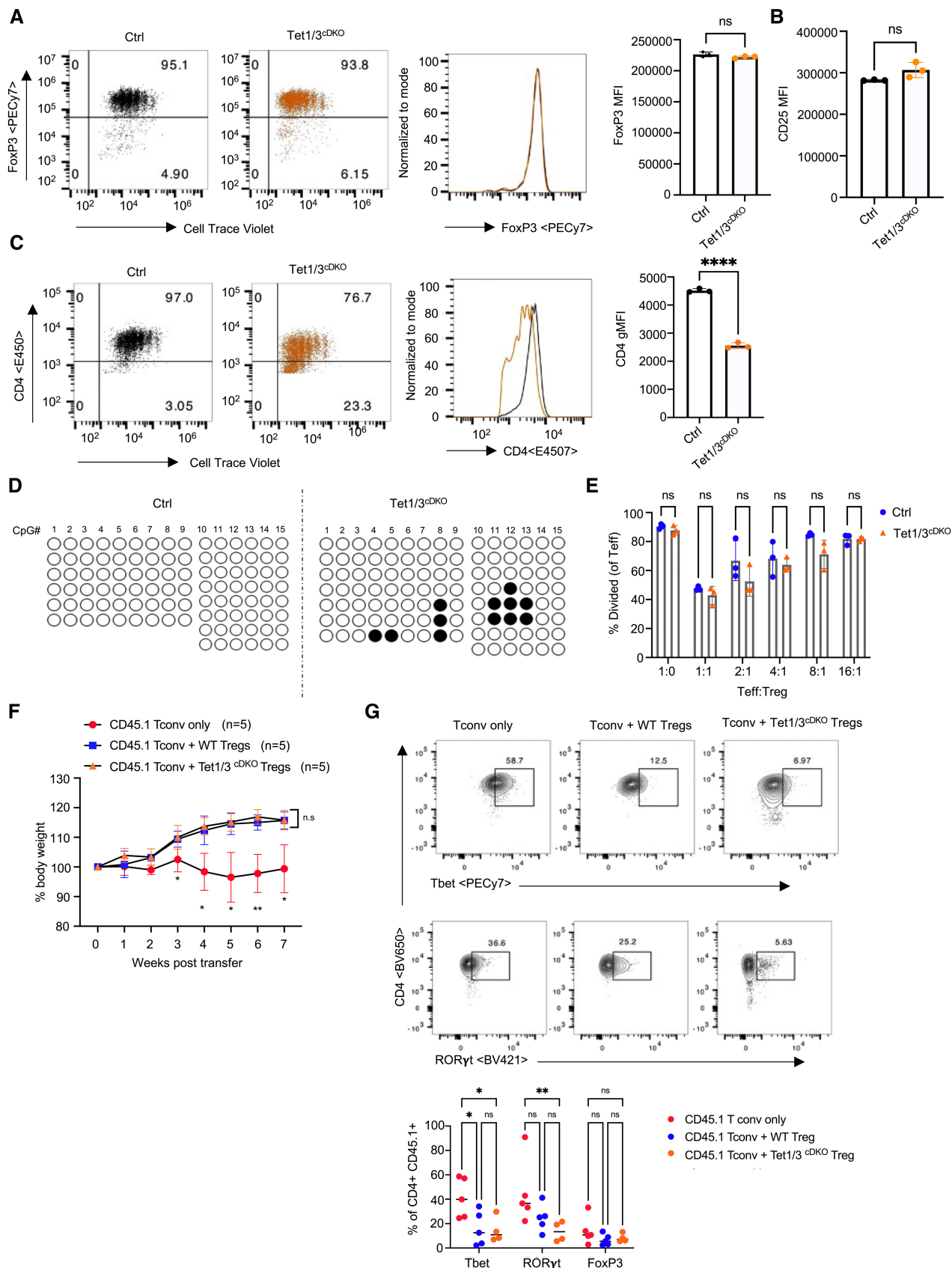Source data are available online for this figure.

Figure 2.

although future studies comparing the whole genome transcriptomic profiles of effector Tet1/3[cDKO] Tregs are warranted. Together these data indicate that unlike Tet2/3[cDKO] Tregs which exhibit defects in Treg cell maintenance and function (Yue *et al*, 2016, 2019), Tet1/3[cDKO] Treg cells are transcriptionally stable and highly functional upon activation.

Tet1 and 3 are required prior to lineage commitment of Treg cells from CD4^{+} T lymphocytes

Given the reduced Treg cell numbers in Tet1/3-deficient mice despite the normal maintenance of Treg cells, we hypothesized that Tet1/3 regulate Treg cell lineage differentiation from CD4^{+} T cells. We first examined the CD4 versus Treg-specific requirement for Tet1/3 by utilizing *Tet1/3[fl/fl]* mice crossed to a *Foxp3*[YFPCre] driver (Rubtsov *et al*, 2008) and generated mice in which *Tet1/3* alleles are deleted upon FoxP3 expression (*Foxp3[Cre] Tet1/3[fl/fl]*). In sharp contrast to *Rorc(t)*[CreTg] *Tet1/3[fl/fl]* mice, *Foxp3[Cre] Tet1/3[fl/fl]* mice displayed no differences in their Treg cell proportions and absolute numbers in the thymus, spleen, or mesenteric lymph nodes compared with littermate controls (Fig 3A and B), suggesting that Tet1/3 are required prior to FoxP3 induction in Treg cells. We thus postulated that Tet1/3 are required early during lineage differentiation of Treg cells in the thymus. To test this, we first excluded a potential confounding role for circulating Tregs, which make up a significant fraction of CD25^{+}FoxP3^{+} Treg cells in the thymus (Thiault *et al*, 2015). However, even after exclusion of CD73^{+} circulating CD4^{+} T cells in the thymus (Owen *et al*, 2018; Darrigues *et al*, 2021), Tet1/3[cDKO] mice had significantly lower CD25^{+}FoxP3^{+} Treg cells than control littermates (Fig 3C), further underscoring a putative developmental defect. As TCR signaling plays a vital role in promoting Treg differentiation (Li & Rudensky, 2016), we investigated whether differences in TCR signaling following maturation of DP thymic

precursors could be altered in Tet1/3[cDKO] mice. We measured Nur77 expression, which correlates with strength of TCR signaling *in vivo* (Moran *et al*, 2011), in TCR-signaled CD69^{+} TCRβ^{hi} CD4^{+} thymocytes and found significantly reduced Nur77 expression in Tet1/3[cDKO] T cells compared with controls (Fig 3D). Examination of CD24 expression in developing thymocytes, a marker of T cell maturity (Tani-ichi *et al*, 2013), revealed no significant differences (Fig EV2A), suggesting that maturation of thymocytes following positive selection was unlikely to be defective in these mice. Additionally, no gross differences in apoptosis among TCRβ[hi] thymocytes, assessed by Annexin V/PI as well as pan-caspase FLICA staining (Fig EV2B), were seen.

To better characterize the differentiation defect, we examined two types of thymic Treg cell precursors, namely CD25^{+}FoxP3^{−} and CD25^{−}FoxP3^{lo} cells, which were recently shown to arise by distinct development pathways and to give rise to Treg cells with differential effector properties (Owen & Farrar, 2019). Intriguingly, Tet1/3[cDKO] adult as well as day-6 neonatal mice had a significant reduction in CD25^{−}FoxP3^{lo} precursors but not CD25^{+}FoxP3^{−} precursors (Figs 3E and F, and EV2C) Consistent with a stronger and/or recent TCR signaling experienced by CD25^{+}FoxP3^{−} cells (Marshall *et al*, 2014; Owen & Farrar, 2019), CD25^{+}FoxP3^{−} cells expressed higher levels of Nur77 compared to CD25^{−}FoxP3^{lo} cells (Fig 3G). However, both control and Tet1/3[cDKO] CD25^{+}FoxP3^{−} and CD25^{−}FoxP3^{lo} precursor cells exhibited comparable Nur77 expression (Fig 3G). To determine whether the defect in thymic Treg development was dependent on both Tet1 and Tet3, we utilized Tet1 and Tet3 single conditional knockout mice. Similar to Tet1/3[cDKO] mice, Tet3[cKO] mice, but not Tet1[cKO] mice, had a significant reduction in CD25^{−}FoxP3^{lo} precursors and CD25^{+}FoxP3^{+} thymic Treg cells but no defect in CD25^{+}FoxP3^{−} precursors (Fig 3H and I). Furthermore, TCR-signaled CD69^{+} TCRβ^{hi} CD4^{+} Tet3[cKO], but not Tet1[cKO] thymocytes also displayed lower Nur77 expression compared with WT controls (Fig 3J and K). These data highlight a dominant and nonredundant role for Tet3

Figure 3. Tet1 and 3 are required prior to lineage commitment of Treg cells from CD4^{+} T lymphocytes.

A   Representative flow plot and quantification of percent FoxP3^{+} cells among Live CD4^{+} T cells in different organs of *FoxP3[Cre] Tet1/3[+/+]* (*n* = 6 biological replicates) and *FoxP3[Cre] Tet1/3[fl/fl]* (*n* = 4 biological replicates) male littermate mice. Data are shown as mean ± SEM, one-way ANOVA with uncorrected Fisher's LSD test.

B   Quantification of Live CD4^{+} FoxP3^{+} T cells absolute cell numbers in different organs of *FoxP3[Cre] Tet1/3[+/+]* (*n* = 3 biological replicates) and *FoxP3[Cre] Tet1/3[fl/fl]* (*n* = 3 biological replicates) male littermate mice. Data are shown as mean ± SEM, one-way ANOVA with uncorrected Fisher's LSD test.

C   Representative flow plot showing gating strategy and quantification of mature CD73- CD25^{+} FoxP3^{+} Tregs in the thymus of control *Tet1/3[fl/fl]* (*n* = 6 biological replicates) and *Rorc(t)*[CreTg] *Tet1/3[fl/fl]* (*n* = 6 biological replicates) mice. Data are shown as mean ± SEM, unpaired two-tailed Mann–Whitney *t*-test.

D   Representative histogram plot (left) and quantification of Nur77 staining (right) among TCRβ^{hi} CD69^{+} CD4 SP thymocytes from control *Tet1/3[fl/fl]* (*n* = 5 biological replicates) and *Rorc(t)*[CreTg] *Tet1/3[fl/fl]* mice (*n* = 6 biological replicates). Dotted line represents staining on TCRβ^{lo}CD4^{+}CD8^{+}CD69^{−} preselected DP thymocytes. Data are shown as mean ± SEM, unpaired two-tailed Mann–Whitney *t*-test.

E   Representative flow plots of CD25^{−}FoxP3^{lo}, CD25^{+}FoxP3^{−} precursor cells and CD25^{+}FoxP3^{+} cells among Live CD4^{+} T cells thymocytes of control *Tet1/3[fl/fl]* (*n* = 6 biological replicates) and *Rorc(t)*[CreTg] *Tet1/3[fl/fl]* mice (*n* = 4 biological replicates).

F   Quantification of cell populations in (E). Data are shown as mean ± SEM, two-way ANOVA with uncorrected Fisher's LSD test.

G   Quantification of Nur77 MFI on indicated precursor populations in the thymus of control *Tet1/3[fl/fl]* (*n* = 5 biological replicates) and *Rorc(t)*[CreTg] *Tet1/3[fl/fl]* mice (*n* = 4 biological replicates). Data are shown as mean ± SEM, two-way ANOVA with Sidak's multiple comparison test.

H   Quantification of CD25^{−}FoxP3^{lo}, CD25^{+}FoxP3^{−}, and CD25^{+}FoxP3^{+} cells among Live CD73^{−}CD4^{+} T cells thymocytes of control *Tet3^{fl/fl}* (*n* = 5 biological replicates) and *Rorc(t)*[CreTg] *Tet3^{fl/fl}* (*n* = 3 biological replicates) mice. Data are shown as mean ± SEM, two-way ANOVA with Sidak's multiple comparison test.

I   Quantification of CD25^{−}FoxP3^{lo}, CD25^{+}FoxP3^{−}, and CD25^{+}FoxP3^{+} cells among Live CD73^{−}CD4^{+} T cells thymocytes of control *Tet1^{fl/fl}* (*n* = 6 biological replicates) and *Rorc(t)*[CreTg] *Tet1^{fl/fl}* mice (*n* = 6 biological replicates). Data are shown as mean ± SEM, two-way ANOVA with Sidak's multiple comparison test.

J   Quantification of Nur77 staining among TCRβ^{hi} CD69^{+} CD4 SP thymocytes from control *Tet3^{fl/fl}* (*n* = 5 biological replicates) and *Rorc(t)*[CreTg] *Tet3^{fl/fl}* mice (*n* = 3 biological replicates). Data are shown as mean ± SEM, unpaired two-tailed Mann–Whitney *t*-test.

K   Quantification of Nur77 staining among TCRβ^{hi} CD69^{+} CD4 SP thymocytes from control *Tet1^{fl/fl}* (*n* = 4 biological replicates) and *Rorc(t)*[CreTg] *Tet1^{fl/fl}* mice (*n* = 3 biological replicates). Data are shown as mean ± SEM, unpaired two-tailed Mann–Whitney *t*-test.

Data information: ns = not significant, *P < 0.05, **P < 0.01, ***P < 0.001, ****P < 0.0001. For (C–K), paired male or female mice were used and no gender biases associated with genotypes were observed. (A–H) Data were replicated >3 times. (I, K) Data were replicated two times.
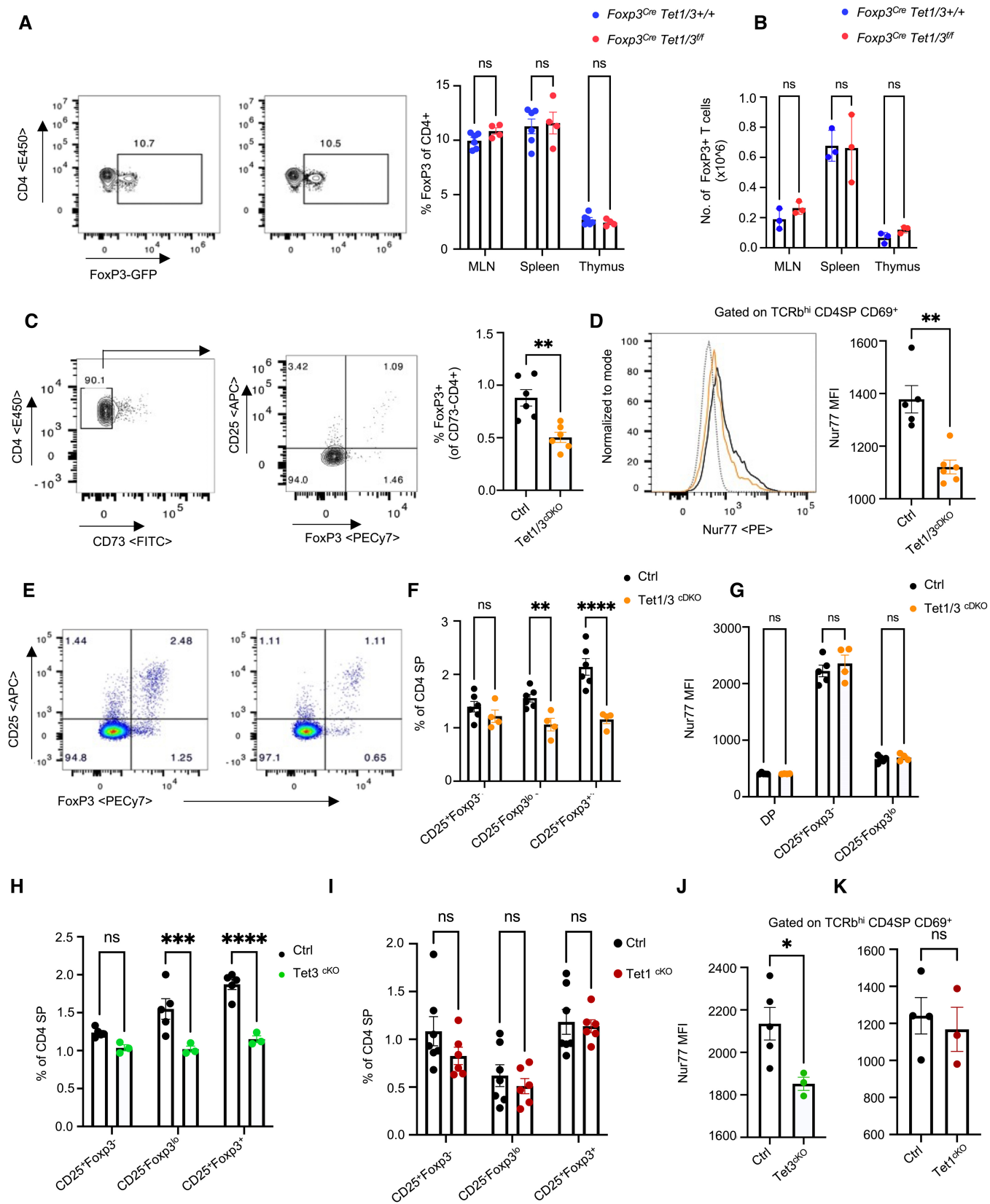Source data are available online for this figure.

Figure 3.

in the development of CD25^{+}FoxP3^{lo} and mature Treg cells. Intriguingly, however, ICOS expression was comparable in both Tet1[cKO] and Tet3[cKO] Treg cells (Fig EV2D and E), suggesting that Tet1 control important transcriptional nodes in mature Treg cells together with Tet3.

Tet1 and 3 regulate Treg differentiation by modulating TCR signaling and IL-2 production

To identify the molecular mechanisms by which Tet1/3 regulate Treg differentiation, we modeled Treg cell differentiation *in vitro* (iTregs) through TCR-mediated activation of naïve CD4^{+} T cells in the presence of TGF-β and IL-2, all of which are signals that drive Treg differentiation *in vivo* (Fantini *et al*, 2004; Zheng *et al*, 2007; Li & Rudensky, 2016). We first explored whether Tet1/3[cDKO] CD4^{+} T were differentially responsive to TGF-β stimulation during iTreg cell differentiation. Compared with WT controls, Tet1/3[cDKO] CD4^{+} T cells were equally able to differentiate into FoxP3^{+} iTreg cells in response to titrated doses TGF-β in IL-2 sufficient conditions (Fig EV3A). Remarkably, however, Tet1/3[cDKO] CD4^{+} T cells were dependent on exogenous IL-2 for optimal differentiation relative to WT controls (Fig 4A). Tet1/3[cDKO] iTreg differentiation could be rescued by the addition of increasing doses of exogenous IL-2, which increased FoxP3 expression, (Figs 4A and EV3B and C) in agreement with a role for IL-2 in modulating FoxP3 expression (Fontenot *et al*, 2005; Burchill *et al*, 2007). Notably, *Foxp3*[Cre] *Tet1/3*[fl/fl] CD4^{+} T cells showed no impairment in their ability to differentiate into iTreg cells *in vitro* in the absence of IL-2 compared with controls (Fig EV3D), underlining the requirement of Tet1/3 prior to FoxP3 expression.

Next, we asked whether IL-2 produced early upon CD4^{+} T cell activation plays a key role during iTreg differentiation and whether IL-2 production is impaired in the absence of Tet1/3. Congruent with this idea, IL-2 protein and mRNA levels were significantly reduced in activated Tet1/3[cDKO] CD4^{+} T cells (Fig 4B and C). Upon activation, both the proportion of IL-2-producing cells and the amount of IL-2 produced per cell were lower in Tet1/3[cDKO] CD4^{+} T cells as determined by flow cytometry (Fig 4D and E). As IL-2 production is actively suppressed by FoxP3 and TGF-β (McKarns *et al*, 2004; Bettelli *et al*, 2005; Fontenot & Rudensky, 2005; Wu *et al*, 2006), we also measured IL-2 production in the presence of TGF-β 48-h post-TCR activation, at which time point FoxP3 is moderately expressed. While we observed a significant decrease in IL-2 production by WT CD4^{+} T cells in the presence of TGF-β, IL-2 was still detectable and significantly lower in Tet1/3[cDKO] CD4^{+} T cells compared with WT controls (Fig 4F). In spite of reduced IL-2 production, it is worthwhile noting that Tet1/3[cDKO] CD4^{+} T cells had no defect in proliferation as assessed by CFSE labeling, under normal or iTreg-specific conditions (Fig EV3E) in agreement with a dispensable role of IL-2 for early T cell proliferation *in vitro* (Popmihajlov *et al*, 2012). To confirm the autocrine/paracrine role of IL-2 in iTreg differentiation, naïve WT CD4^{+} T was activated in the presence of an anti-IL-2 blocking antibody. In keeping with the critical need for IL-2 during iTreg differentiation (Davidson *et al*, 2007; Zheng *et al*, 2007), blockade of murine-derived IL-2 completely abrogated

---

Figure 4. Tet1 and 3 regulate Treg differentiation by modulating TCR signaling and IL-2 production.

A Quantification of % FoxP3^{+} cells 72-h postactivation of sorted naïve CD4^{+} T cells with anti-CD3/CD28 and 20 ng/ml TGF-β in the presence or absence of indicated amounts of rhIL-2 for 72 h (*n* = 3 biological replicates per dose). Data are shown as mean ± SEM of three independent samples, two-way ANOVA with uncorrected Fisher's LSD test.

B IL-2 quantification by ELISA in supernatants collected at indicated time points following activation of sorted naïve CD4^{+} T cells with anti-CD3/CD28 and without exogenous IL-2 or TGF-β (*n* = 8 biological replicates). Data are shown as means ± SEM of eight independent samples from two mice/genotype. Two-way ANOVA with uncorrected Fisher's LSD test.

C IL-2 mRNA quantification by qPCR in CD4^{+} T cells postactivation at indicated time points (*n* = 2 biological replicates/genotype). Cells were stimulated with anti-CD3/CD28 without exogenous IL-2 or TGF-β. Data are shown as mean ± SEM, two-way ANOVA with Sidak's multiple comparison test.

D Representative flow plots of IL-2 expression by flow cytometry in CD4^{+} T cells, 48-h postactivation with anti-CD3/CD28 (*n* = 3 biological replicates). Cells were treated with Monensin + Brefeldin A for the last 6 h.

E Quantification of (D). Data are shown as mean ± SEM of three independent samples, unpaired two-tailed Mann–Whitney *t*-test.

F IL-2 quantification by ELISA in supernatants collected at 48-h postactivation of naïve CD4^{+} T cells with anti-CD3/CD28 without exogenous IL-2 and in the presence or absence of 20 ng/ml TGF-β (*n* = 4 biological replicates). Data are shown as mean ± SEM, two-way ANOVA with Bonferroni's multiple comparison test.

G % CD25^{+}FoxP3^{+} among FoxP3^{+} cells generated after sort-purified mature CD4SP from control *Tet1/3*[fl/fl] and *Rorc(t)*[CreTg] *Tet1/3*[fl/fl] Foxp3 reporter mice were stimulated with or without plate-bound anti-CD3/CD28 for 10–12 h and then replated in fresh medium or in their conditioned medium (cond. medium) or in the presence of rhIL-2 for an additional 12 h (*n* = 3–6 biological replicates/genotype).

H IL-2 quantification by ELISA in supernatants collected at 12-h postactivation of sort-purified mature CD4SP thymocytes (*n* = 4 biological samples). Data are shown as mean ± SEM, unpaired two-tailed Mann–Whitney *t*-test.

I DNA methylation assessment by amplicon-based bisulfite sequencing of CpG sites at the IL-2 promoter of activated control *Tet1/3*[fl/fl] and *Rorc(t)*[CreTg] *Tet1/3*[fl/fl] CD4^{+} T cells. Cells were stimulated with anti-CD3/CD28 without exogenous IL-2 or TGF-β for 72 h, and DNA was isolated for analysis.

J Representative flow plot and quantification of Nur77 expression in CD4^{+} T cells activated for 18 h with anti-CD3/CD28 in the absence of exogenous IL-2 or TGF-β. Dotted line is nonspecific staining control. Data shown are representative of >2 independent experiments and shown as mean ± SEM of three independent samples, one-way ANOVA with Bonferroni multiple comparison tests.

K IL-2 quantification by ELISA in supernatants collected at 5-h postactivation of naïve CD4 T cells with PMA/Ionomycin (*n* = 7). Data are shown as mean ± SEM, two-way ANOVA with Sidak's multiple comparison test.

L IL-2 quantification by ELISA in supernatants collected at 72 h following activation of CD4 T cells with anti-CD3/CD28 without exogenous IL-2 or TGF-β (*n* = 3). Data are shown as mean ± SEM, one-way ANOVA with Tukey's multiple comparison test.

M, N Quantification of % FoxP3^{+} cells among CD4 T cells 72-h activation with anti-CD3/CD28 and 20 ng/ml TGF-β in the presence or absence of 50 U rhIL-2 for 72 h (*n* = 3 biological replicates). Data are shown as mean ± SEM, one-way ANOVA with Tukey's multiple comparison test.

Data information: *P < 0.05, **P < 0.01, ***P = 0.001, ****P < 0.0001. Male and female mice were used in (A–N), and no gender biases associated with genotypes were observed. (A–J, M, N) Data were replicated >3 times; (K, L) data were replicated two times.
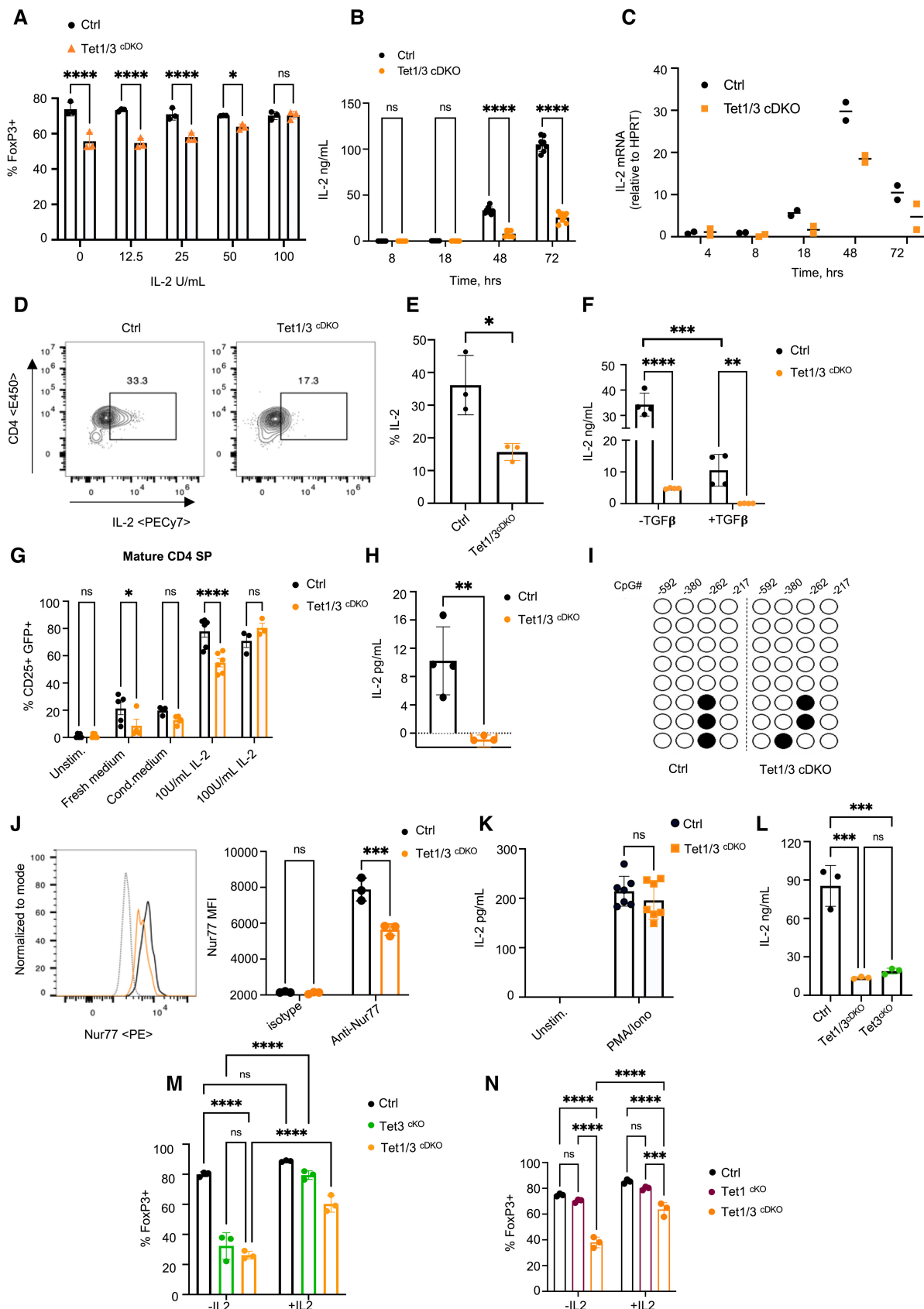Source data are available online for this figure.

Figure 4.

FoxP3$^+$ iTreg cell differentiation and could be partially rescued via the addition of exogenous human rIL-2 (Fig EV3F).

We also examined whether an IL-2-dependent mechanism was responsible for the reduction of thymic Treg cell numbers in Tet1/3^{cDKO} mice. Previous work has shown that T cells are a critical source of IL-2 during thymic Treg differentiation (Owen *et al*, 2018) and more recently, using integrated IL-2 fate mapping, transcriptomic profiling and an *in vitro* model of thymic Treg differentiation, it was elegantly shown that upon TCR stimulation and exposure to autocrine or paracrine IL-2, immature and mature thymic CD4SP cells could upregulate FoxP3 protein expression, supporting a model where Treg precursor cells can promote their own differentiation into Treg cells in an IL-2 and TCR-dependent manner (Hemmers *et al*, 2019). In addition to similar findings in our study, we found that mature CD4SP thymocytes from Tet1/3^{cDKO} mice were more impaired to differentiate into CD25$^+$ FoxP3$^+$ Treg cells than WT counterparts, but such defect could be partially rescued in the presence of excess IL-2 (Fig 4G). Correspondingly, upon stimulation mature CD4SP thymocytes from Tet1/3^{cDKO} mice produced less IL-2 than WT controls (Fig 4H).

The IL-2 promoter has previously been shown to undergo active promoter demethylation during TCR activation, although the enzyme/s mediating this process have not been identified (Bruniquel & Schwartz, 2003). We therefore tested whether IL-2 promoter demethylation was mediated via Tet1 and 3. To our surprise, the IL-2 promoter from both activated WT and Tet1/3-deficient CD4$^+$ T cells underwent similar loss in DNA methylation at previously reported CpGs (Fig 4I), suggesting that Tet1/3 were not required for promoter demethylation of the *Il-2* gene. However, we found reduced levels of Nur77 expression in TCR-activated Tet1/3-deficient CD4$^+$ T cells, suggestive of reduced strength of TCR signaling (Fig 4J). Importantly, Tet1/3-deficient CD4$^+$ T cells produced comparable levels of IL-2 upon short-term PMA/Ionomycin stimulation, indicating that Tet1/3-deficient CD4 T cells do not have an intrinsic defect in IL-2 production, but likely respond differently to anti-CD3/CD28-driven TCR stimulation (Fig 4K). Strikingly, IL-2 production was highly dependent on Tet3 as CD4$^+$ T cells from Tet3^{cKO} produced significantly reduced IL-2 (Fig 4L) and showed significantly impaired iTreg differentiation, which could be rescued by provision of exogenous IL-2 (Fig 4M) while Tet1 deficiency alone had no impact on iTreg differentiation (Fig 4N).

Tet1 and 3-dependent IL-2 secretion shapes the early chromatin landscape of differentiating Tregs

To determine the impact of reduced IL-2 autocrine signaling in Tet1/3-deficient differentiating iTregs, we first confirmed a reduction in IL-2-dependent signaling by probing for phosphorylated Stat5 (pStat5), a key transcriptional regulator immediately downstream of IL-2 signaling (Gilmour *et al*, 1995). Consistent with reduced autocrine IL-2 signaling, Stat5 phosphorylation was significantly blunted in Tet1/3^{cDKO} CD4$^+$ T cells compared with WT controls. pStat5 expression was decreased in Tet1/3^{cDKO} CD4$^+$ T cells but could be rescued in the presence of exogenous IL-2 (Fig 5A), supporting the idea that autonomous IL-2 plays a critical role in Treg differentiation.

To look at the global chromatin landscape in differentiating iTregs, we performed an assay for Transposase-Accessible Chromatin using sequencing (ATAC-Seq; Buenrostro *et al*, 2013). In the absence of IL-2, differentiating Tet1/3^{cDKO} iTreg cells showed a significant reduction in the proportion of open regions at key genes such as *IL-2*, *Socs3*, *St5*, *ICOS*, and TCR-related genes such as *Fyn*, *Lck*, *Cd4*, *Nfatc2*, and *Itk* compared with control cells (Fig 5B). Gene ontology enrichment analysis revealed that the most significantly enriched and differential gene targets were integral players of the IL-2 and TCR signaling pathways (Fig 5C, Dataset EV1) and included proximal TCR genes such as *Lck* (Fig 5D), *Fyn* (Fig 5E), and *Itk* (Fig 5F), whereby differentially accessible peaks mapping to noncoding regions of the gene loci were observed and not restored in the presence of IL-2. Intriguingly, although DNA methylation marks at the IL-2 gene promoter in WT and Tet1/3^{cDKO} CD4$^+$ T cells were unimpaired, we observed reduced chromatin accessibilities at the promoter as well as at a putative enhancer site within the IL-2 locus (Fig 5G), suggesting that pathways downstream of TCR signaling and leading to IL-2 transcription are likely affected. In agreement with a dual role for TCR and IL-2 signaling impeding iTreg differentiation of Tet1/3^{cDKO} CD4$^+$ T cells, the top three significantly enriched consensus motifs within differentially accessible peaks belonged to JunB, ETS, and Stat5 transcription factors (Fig 5H). The putative enhancer site within the IL-2 locus also contained binding sites for JunB and ETS, suggesting a putative TCR-dependent regulation of this region. Pearson correlations between chromatin accessibility profiles showed that the chromatin accessibility landscape of

---

Figure 5. Tet1 and 3-dependent IL-2 secretion shapes the early chromatin landscape of differentiating Tregs.

A Representative flow plots (top) and quantification of phosphoStat5 MFI expression (bottom) in CD4$^+$ T cells, 18-h postactivation with anti-CD3/CD28 and ±20 ng/ml TGF-β or ±100 U rhIL-2 (*n* = 2 or 3). Data were replicated >3 times.

B Scatter plot depicting regions in CD4$^+$ T cells with differences in chromatin accessibility between *Rorc(t)^{CreTg} Tet1/3$^{fl/fl}$* and WT controls. Gray points indicate no difference in accessibility (FDR > 0.05 or FDR < 0.05, Log2 (cDKO/WT) < Log2 (1.5)) and red points indicate increased accessibility in DKO CD4$^+$ T (FDR < 0.05, Log2 (cDKO/WT) < −Log2 (1.5)) and blue points indicate decreased accessibility in DKO CD4$^+$ T cells (FDR < 0.05, Log2 (cDKO/WT) < −Log2 (1.5)). T cells were activated for 48 h with anti-CD3/CD28 and 20 ng/ml TGF-β but no IL-2. DKO = *Rorc(t)^{CreTg} Tet1/3$^{fl/fl}$*, *n* = 2 biological replicates/genotype/condition.

C Gene ontology analysis using Enrichr, with most statistically significant enriched ontologies of genes with differential accessibility shown.

D–F Integrated genome viewer (IGV) browser tracks of the *Lck*, *Fyn*, and *Itk* gene loci highlighting differential accessible regions (in red boxes) in biological replicates of CD4$^+$ T cells activated with anti-CD3/CD28 and 20 ng/ml TGF-β ±100 U IL-2.

G IGV browser track of the IL-2 locus showing accessibility peaks at the IL-2 promoter region and upstream of the promoter (red arrow) in biological replicates of CD4$^+$ T cells activated as in (B).

H Motif enrichment analysis of TF binding motifs using the HOMER database, with indicated percentage of target genes containing differential accessibility peaks and enriched in consensus motifs of the JunB, ETS, and Stat5 TF family members shown.

I IGV browser track of the *Foxp3* locus highlighting differential accessibility at the CNS2 region in biological replicates of CD4$^+$ T cells activated with anti-CD3/CD28 and 20 ng/ml TGF-β ±100 U IL-2.
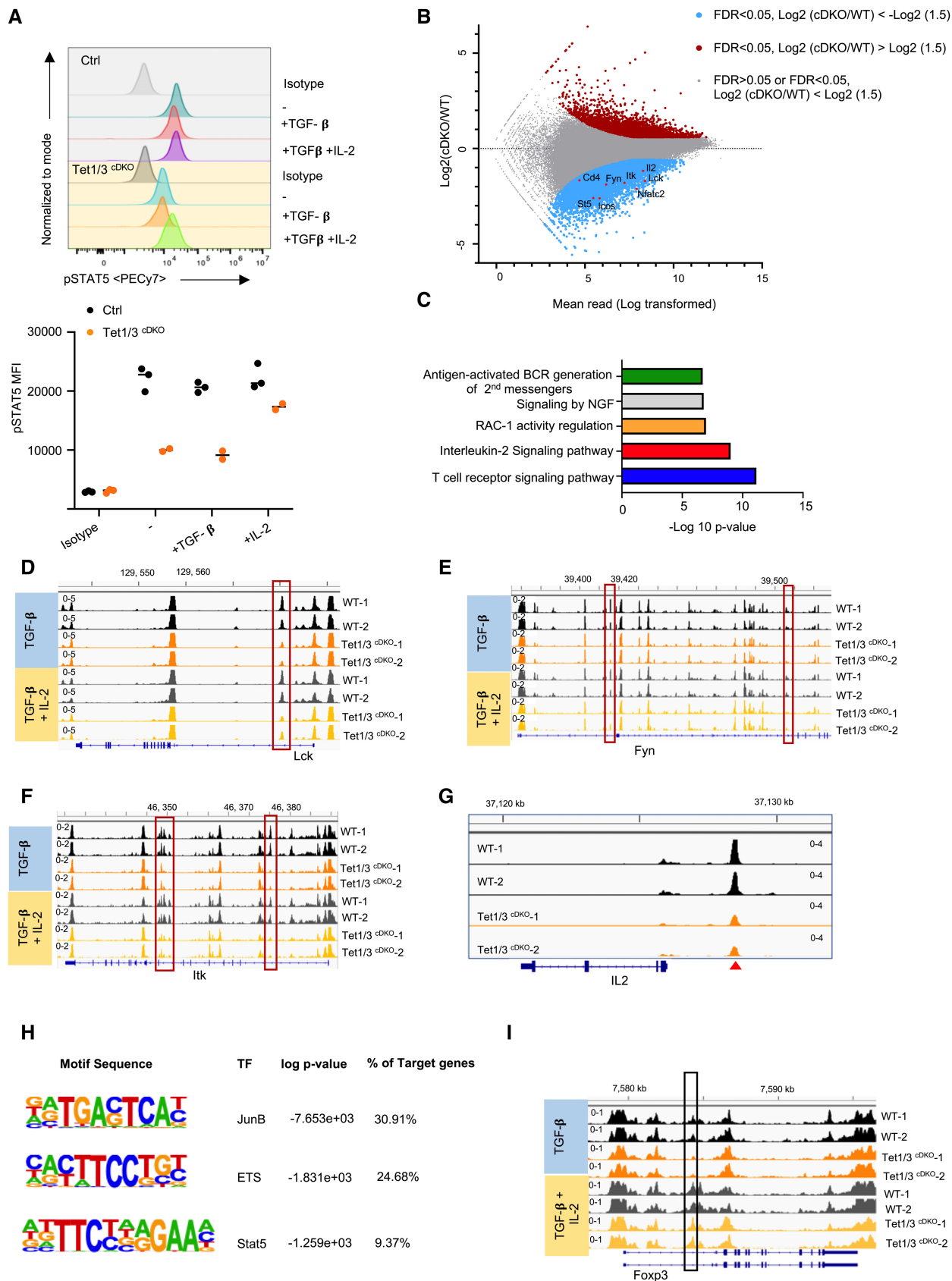
Source data are available online for this figure.

Figure 5.

Tet1/3^{cDKO} CD4$^+$ T cells treated with exogenous IL-2 approached the chromatin accessibility landscape of WT CD4$^+$ T cells (Fig EV4A). Of the 18,696 peaks that were differentially accessible (FDR < 0.05) between TGF-β-treated WT and Tet1/3^{cDKO} CD4$^+$ T cells, only 21% (3,935 peaks) were differentially accessible between TGF-β+IL-2-treated and TGF-β-treated Tet1/3^{cDKO} CD4$^+$ T cells (Fig EV4B). *De novo* motif analysis revealed that 26.45% of those restored peaks were most significantly enriched for Stat5 binding motifs. Importantly, a key gene affected through autonomous IL-2 signaling was *Foxp3* itself, which displayed reduced accessibility within the CNS2 site of the gene, which contains a previously characterized Stat5-binding region (Yao *et al*, 2007), in Tet1/3^{cDKO} CD4$^+$ T cells compared with WT controls, and was restored in the presence of exogenous IL-2 (Fig 5I). Together these data highlight the significance of autonomous IL-2 signaling in the epigenetic programming of iTregs early during differentiation and support a key role for Tet1/3 in the modulation of this process.

In aggregate, our results highlight a novel role for Tet1/3-dependent DNA demethylation in setting up the stage for optimal TCR signaling and IL-2 production in CD4$^+$ T cells early during thymic T cell development, thereby promoting Treg differentiation. However, Tet1/3-deficient Tregs maintained normal suppressive functions and maintained stable transcriptional programs essential for their lineage integrity. Notably, Tet1/3-deficient Tregs expressed normal expression of CD25 and FoxP3 while it was previously shown that Tet2/3-deficient Treg cells have significantly reduced CD25 and FoxP3 expression and consistently, a severe loss of suppressive function *in vivo* (Yue *et al*, 2019). Defects in the IL-2R signaling complex result in impaired survival and function (Chinen *et al*, 2016; Fan *et al*, 2018) and highlight the distinct requirements of the IL2 trimeric receptor as guidance for Treg cells to sense their IL-2-producing T cell targets, and/or Treg cell–mediated deprivation of IL-2 as a key mechanism of suppression. To date, it remains unclear whether epigenetic factors drive the development of Treg cell precursors and this study highlights a critical role of DNA demethylation in the development of CD25$^-$FoxP3^{lo} precursors from CD4$^+$ thymocytes. It was recently shown that the generation of these cells is highly dependent of CD28-mediated co-stimulation and NF-KB1 signaling (Owen & Farrar, 2019). Our findings suggest that TCR signaling strength could also be an important determinant of this developmental pathway and that CD25$^-$FoxP3^{lo} precursors may be more sensitive to altered TCR thresholds and/or IL-2 signaling than CD25$^+$FoxP3$^-$ precursors. It is plausible that DNA demethylation modulates TCR signaling strength by controlling TCR co-stimulation. Given that Nur77 expression in committed CD25$^-$FoxP3^{lo} precursors is not differential in the absence of Tet1 and Tet3, or Tet3 alone, we speculate that high-affinity TCR-expressing cells differentiating along this developmental course are selected and successfully mature into Treg cells. It also remains unclear whether the mature Treg pool in Tet1/3-deficient mice is comprised of fewer CD25$^-$FoxP3^{lo}-derived Treg cells and could explain the increased functional fitness we see *in vivo*, as Treg cells derived from different precursors have recently been shown to have different functional capacities (Owen & Farrar, 2019). Future studies examining the TCR repertoire and co-stimulatory arms of developing Treg cells in Tet1/3-deficient mice will be informative.

Lastly, our study highlights a novel and epigenetically programmed circuit that integrates TCR-mediated signals in a "bottom-up" manner, irrespective of TCR-dependent affinities and avidities. This could have major implications for cell fate decisions in the thymus and in the regulation of self-tolerance in mice and humans. There is currently enormous interest in uncovering epigenetic pathways to induce the generation of transcriptionally stable *in vitro*-derived Tregs for therapy (Sakaguchi *et al*, 2020). However, pathways to promote the differentiation of endogenous Treg cells are lesser understood. Our study thus uncovers a new epigenetic node that could potentially be manipulated to promote the differentiation of Treg cells from CD4$^+$ thymocytes *in vivo* and improve self-tolerance.

Materials and Methods

Mice

Tet1 and *Tet2* floxed (C57BL/6J) and *Tet3* floxed mice (129 backcrossed to C57BL/6J) were kindly provided by Dr. Iannis Aifantis (Moran-Crusio *et al*, 2011) and Dr. Yi Zhang (Shen *et al*, 2014), respectively. These mice were then backcrossed onto *Rorc(t)^{CreTg}* (B6.FVB-Tg(Rorc-cre)1Litt/J #022791) mice and FoxP3$^{YFP-Cre}$ (B6.129(Cg)-*Foxp3$^{tm4(YFP/icre)Ayr}$*/J #016959) mice and Foxp3EGFP (C.Cg-*Foxp3^{tm2Tch}*/J #006769) mice purchased from Jackson Laboratory. B6.SJL-CD45.1 mice (#002014) and B6.129S7- Rag1tm1Mom/J (#002216) mice were purchased from the Jackson Laboratory. All mice were maintained under specific pathogen-free (SPF) conditions at the barrier animal facility at the University of Iowa Carver College of Medicine on a 12-h light cycle at 30–70% humidity and temperature of 20–26°C, with access to standard chow and water. Littermate controls and sex-matched 6–8-week-old mice were used for all experiments unless specified otherwise. CO$_2$ exposure was used as the method for euthanasia for all experiments. Permission for all animal experiments performed was granted by the IACUC at the University of Iowa Carver College of Medicine under protocol number 0011979.

Naïve T cell sorting

Single-cell suspensions were prepared from the spleen or lymph nodes after mashing through 70 μm cell strainers. Red blood cells were lysed in ACK lysis Buffer (Gibco), and a Dynabeads untouched mouse CD4 T cell kit (Thermo Fisher) was used to enrich for CD4$^+$ T cells. Cells were surface stained in IMDM containing 2% FBS for 30 min at 4°. Cells were washed, and naïve CD4$^+$ T cells were then FACS sorted on a BD FACSAria II or FACSAria Fusion cell sorter by gating on CD19$^-$CD25$^-$CD4$^+$CD62L^{hi} CD44$^-$ T cells. Cell purity was verified and estimated to be > 98%.

Flow cytometry analysis

For immune subset profiling, single-cell suspensions were prepared from the thymus, spleen, peripheral lymph nodes, or mesenteric lymph nodes by mashing through 70 μm cell strainers. Red blood cells were lysed in ACK lysis Buffer (Gibco) and counted on a Countess II Automated Cell counter (Thermo Fisher). Cells were surface stained in IMDM containing 2% FBS for 30 min at 4° or 20 min at RT followed by fixation with a Foxp3/Transcription

Factor Staining Buffer Kit (Tonbo). After overnight fixation, cells were permeabilized and stained for FoxP3 or Nur77 at RT for 45 min. For intracellular detection of cytokine production, following stimulation for indicated time points, cells were incubated in the presence of Monensin and Brefeldin A for 5–6 h at 37°, followed by staining of cell surface markers at RT for 20 min. Cells were then fixed in 2% PFA for 15–30 min at 4° and washed two times in PBS. Permeabilization was performed using the Foxp3/Transcription Factor Fix/Perm Diluent (Tonbo), and cells were stained with cytokine antibodies for 45 min at RT. For phospho-STAT5 staining, cells were fixed and permeabilized with 4% PFA followed by ice cold-90% methanol and stained with anti-pY-Stat5 antibody (BD Biosciences). For apoptosis assessment in thymocytes, a Vybrant FLICA Caspase apoptosis assay (Thermo Fisher) or Annexin V-FITC and PI staining kit (BioVision) was used following the manufacturer's instructions. Thymocytes were stained as soon as cell suspensions were obtained. Stained cells were analyzed on a Cytoflex flow analyzer or an LSR-II flow analyzer. Flow jo (v9.9.6, Tree Star) was used for all flow cytometry analysis.

The antibodies used for flow cytometry and cell sorting were purchased from BioLegend, BD Biosciences, Thermo Fisher Scientific, or Tonbo Biosciences, and their clone numbers are CD45.1 (A20), CD45.2 (104), CD4 (RM4-5), CD8α (53–6.7), TCRβ (H57-597), CD24 (M1/69), CD25 (PC61.5), CD19 (1D.3) CD62L (MEL-14), CD44 (IM7), CD69 (H1.2F3), CD28 (37.51), FoxP3 (3G3), IL-2 (JES6-5H3), ICOS/CD278 (7E.17G9), CTLA4 (UC10-4B9), Nur77 (12.14), pSTAT5 (SRBCZX), IFNγ (XMG1.2), TNF (MP6–XT22), IL-17A (17B7), RORγt (Q31-378), Tbet (4B10), IL-10 (JES5-16E3), and GRANZYME B (QA16A02). Ghost dye (Tonbo) was used for exclusion of dead cells.

DSS colitis

Six–eight-week-old *Tet1/3$^{fl/fl}$* or *Rorc(t)^{CreTg} Tet1/3$^{fl/fl}$* littermate male mice received 1.5% DSS in drinking water for 7 days, and the body weight was monitored daily. Severity and inflammation of colitis were assessed based on bodyweight changes and histopathological examination. All mice were kept in a barrier facility at the Carver College of Medicine, University of Iowa, with access to food and water *ad libitum*. Weight was measured in a blinded manner and unblinded after the conclusion of the experiment.

T cell transfer colitis

For induction of chronic colitis by T conv CD4$^+$ T cells, CD45.1$^+$ CD25$^-$CD62L^{hi} CD44^{lo}TCRβ$^+$ naive CD4$^+$ T cells were sort-purified from female B6.SJL mice and adoptively transferred into female *Rag1$^{-/-}$* mice at 0.5 × 10^6 cells per mouse. To test the capacity of T reg cells in suppressing the T cell–induced colitis, TCRβ$^+$CD4$^+$CD25$^+$ T reg cells were sort-purified from 6 to 8-week-old female *Tet1/3$^{fl/fl}$* control or *Rorc(t)^{CreTg}Tet1/3$^{fl/fl}$* littermates and co-transferred with naive CD4$^+$ T cells into female 5-week-old *Rag1$^{-/-}$* mice at 0.25 × 10^6 cells per mouse. The *Rag1$^{-/-}$* recipients were monitored weekly for body weight and signs of colitis. Six to eight weeks later, colons were harvested for histological analysis, and mesenteric lymph nodes were used for phenotypic characterization of donor-derived lymphocytes. We also tested an 8:1 ratio of Teff/Tregs by transferring 0.5 × 10^6 naïve CD4$^+$ T cells and 0.0625 × 10^6

Treg cells and assessed weight loss in mice over time. Experimental groups were not blinded during weight measurements.

Quantitative real-time reverse transcription

DNase I-treated total RNA was prepared from activated T cells using RNeasy RNA isolation kit (Qiagen), and cDNA was synthesized using an iScript cDNA synthesis kit (Biorad). Quantitative PCR was performed using SsoAdvanced Universal SYBR Green supermix (Biorad) and a CFX Connect Real-time PCR detection system (Biorad). The following primers were used for qRT–PCR. IL-2 mRNA: forward 5′-TGAACTTGGACCTCTGCGG-3′ and reverse 5′-TGTGTTGTCAGAGCCCTTTAGT-3′.

In vitro-induced Treg cultures

96-well flat-bottom tissue culture plates were coated with polyclonal goat affinity purified antibody to hamster IgG (MP Biomedical) at 37°C for at least 2 h or overnight at 4°C and washed 2× with PBS before cell plating. FACS-sorted CD4$^+$CD8$^-$CD25$^-$CD62L$^+$CD44^{lo} naïve T cells were seeded in complete T cell medium [RPMI 1640 (Gibco), 10% heat-inactivated FBS (Gibco Lot no. 2261598RP or Atlanta Lot no. A16003), 2 mM L-glutamine, 50 μg/ml gentamicin, 1% Penn/Strep, 50 μM 2-mercaptoethanol (Gibco)] along with anti-CD3 (Tonbo, clone 17A2, 0.25 μg/ml) and anti-CD28 (Tonbo, clone 37.51, 1 μg/ml) antibodies. TGF-β and IL-2 were provided as indicated in the figure legends. Seventy-two hours later, cells were lifted off the plates and rested for 30 min followed by staining for flow cytometry analysis.

In vitro suppression assays

CD4$^+$CD25$^+$ Tregs from *Rorc(t)^{CreTg}Tet1/3$^{fl/fl}$* or littermate controls were FACS sorted on a BD FACSAria II or FACSAria Fusion cell sorter following enrichment of CD25$^+$CD4$^+$ T cells with anti-PE beads (Miltenyi). Naïve conventional CD4$^+$ T cells were sorted as described previously. Antigen-presenting cells were obtained from the spleen of B6.SJL mice or WT C57BL/6J mice by depletion of CD4$^+$ and CD8$^+$ T cells using a mouse T cell isolation kit (Dynabeads) followed by X-ray irradiation. Tregs were CFSE-labeled, while T conv cells were labeled with a Cell-trace Violet dye. APCs were plated in round-bottom plates at 60,000 cells/well along with 30,000 Tregs and varying ratios of Teff (30,000–480,000 cells) and 1 μg/ml anti-CD3. Cultures were assessed for proliferation 72 h later.

In vitro activation of natural Tregs

96-well flat-bottom tissue culture plates were coated with polyclonal goat affinity purified antibody to hamster IgG (MP Biomedical) at 37°C for at least 2 h or overnight at 4°C and washed 2× with PBS before cell plating. FACS-sorted CD25$^+$FoxP3^{GFP+} Tregs cells, pooled from the spleen and MLN of *Rorc(t)^{CreTg}Tet1/3$^{fl/fl}$* Foxp3^{GFP} mice or littermate controls, were CTV/CFSE-labeled (Thermo Fisher Scientific) and seeded in complete T cell medium along with anti-CD3 (Tonbo, clone 17A2, 0.25 μg/ml) and anti-CD28 (Tonbo, clone 37.51, 1 μg/ml) antibodies and 200 U/ml of rhIL-2. Seventy-two hours later, cells were lifted off the plates and rested for 30 min followed by staining for flow cytometry analysis. For measurements

of cytokines, cells were activated for 48 h similarly as described previously, with the addition Monensin A/Brefeldin A for 5–6 h before processing for flow cytometry.

In vitro activation of CD4SP thymocytes

Thymi from $Rorc(t)^{CreTg}Tet1/3^{fl/fl}$ Foxp3^{GFP} and littermate male mice were dissected and dissociated into a single-cell suspension. Cells were resuspended in IMDM containing 2% FBS and enriched for CD4SP thymocytes by depleting CD8SP and double-positive cells using the anti-CD8PE staining and anti-PE bead depletion (Cell Stem Cell). The enriched cells were stained with fluorochrome-conjugated anti-TCRβ, anti-CD4, anti-CD24, anti-CD25, and anti-CD8 before sorting on a BD FACSAria II sorter. *In vitro* T reg cell induction assay was set up with 3×10^4 of immature and mature CD4 SP cells per well of a flat-bottom 96-well tissue culture plate. The 96-well plates had been coated with anti-CD3 and anti-CD28 at 1 μg/ml in DPBS for 12 h at 4°C or left untreated. Cells were cultured in T cell medium (supplemented RPMI 1640) for 10–12 h in those plates and then transferred to U-bottom 96-well plates and resuspended in fresh T cell medium supplemented with recombinant human IL-2 at the indicated concentrations or resuspended in their own media (conditioned media) for an additional 12 h.

ELISA

IL-2 measurements in the supernatants were performed using a BD OptEIA mouse IL-2 ELISA Set (BD Biosciences) following the manufacturer's instructions. Supernatants from anti-CD3/CD28-activated T cells were diluted between 50 and 100-fold in PBS prior to the ELISA, and undiluted supernatants from unstimulated T cells were used as controls. ELISAs were read at OD450 on a Synergy HTX instrument (BioTek). IL-2 levels were calculated through extrapolation from a standard curve using Excel.

Pyromark bisulfite sequencing

Genomic DNA was isolated from FACS-sorted T cell populations using genomic DNA isolation kits (Qiagen). Purified genomic DNA was subjected to bisulfite treatment with the Qiagen EpiTect bisulfite kit, and regions of interest were PCR-amplified using the Pyromark Bisulfite PCR Kit (Qiagen) and cloned into TA vectors. Bacteria were transformed, and single colonies were isolated, expanded, and miniprepped. Plasmids were then sequenced by Sanger sequencing. Primers used for PCR amplification are as follows: *IL-2* region 1 Forward 5′-ATTTTTTTTGTTTAATTAATAAA TTTAAAA-3′ and Reverse 5′-AAATTTAAATAAAATCCCTCTTAATC-3′; *IL-2* region 2 Forward 5′-TGATTTTTATAGGTGTATTGTGG TATATAT-3′ and Reverse 5′-CCAACAAATTCTCAAAAAAAATTAC AT-3′; *IL-2* region 3 Forward 5′-TGTAATTTTTTTTGAGAATTTGTT GG-3′ and Reverse 5′-CACAAAATAATAAATAACTTCATACAATTA-3′. Primers used for CNS2 methylation assessed were the same as previously published (Yue *et al*, 2016).

Histology

Tissues were harvested and placed in 10% neutral buffered formalin for 3–5 days. The fixed tissues were then processed (dehydrated

through a series of progressive alcohols and xylene baths), paraffin embedded, sectioned at ~4 μm onto glass slides, and stained with hematoxylin and eosin (H&E). Tissues were evaluated by a boarded pathologist using the postexamination method of masking to limit bias in tissue analysis (Meyerholz & Beck, 2018). General organ inflammation was evaluated using severity grade (0 none to 3 severe). Intestinal tissue scoring tiers (0–3) were adapted from a previous publication for tissue inflammation (0—none, 1—mucosal only, 2—mucosa and submucosa, and 3—transmural; Erben *et al*, 2014; Meyerholz & Beck, 2018). For inflammation evaluation, each tiered grade was multiplied by the percent (%) of the tissue affected, summed for each case, and divided by 100 to yield a modified H-Score. Pathologist was blinded to experimental hypothesis.

Preparation of ATAC-Seq libraries

ATAC-Seq was performed using 90,000 cells/sample. Briefly, T cells were rested for 20 min after activation in T cell medium and pelleted at 500 g for 10 min. Cells were washed in 1× DPBS and processed using an ATAC-Seq Kit (Active Motif) following the manufacturer's protocol. After purification of tagmented DNA, a quantitative PCR on the tagmented DNA product determined that on average 7 cycles were required. The library was purified, and size selected two times with Agencourt AMPure beads to remove > 2,000-bp fragments and excess primers. Samples underwent quality control and quantification on an Agilent BioAnalyzer by the Iowa Genomics Operation core at the University of Iowa before pooling and sequencing on an Illumina HiSeq.

Bioinformatics processing and analysis

Sequencing adapters were removed from paired-end reads using Trimmomatic version 0.39 (Bolger *et al*, 2014). Trimmed reads were aligned to mouse reference genome GRCm38 using Bowtie 2 version 2.4.1 with options --very-sensitive -X 2000. Following genome alignment, Picard was used to mark PCR duplicates, and samtools version 1.3.1 was used to remove PCR duplicates, discordant pairs, and alignments to the mitochondrial genome. Peak calling was performed using MACS2 version 2.2.7.1, and differential accessibility analyses of MACS2 peaks were performed using the R package *DiffBind* version 2.10.0. Differentially accessible peaks were annotated to genome regions of interest using the R package *ChIPseeker* version 1.18.0, and sequence motif enrichment analyses were performed using HOMER version 4.11.1. Gene ontology analysis was performed using Enrichr (Kuleshov *et al*, 2016).

Statistical analysis

GraphPad Prism (v. 9.0d) was used for all statistical analyses. For comparison between two experimental groups, Student's *t*-test with two-tailed distribution or Mann–Whitney unpaired two-tailed *t*-test was used. For multiple group comparisons, one-way or two-way ANOVA tests were used with indicated multiple comparison testing in the figure legends, to determine the statistical significance between two specific groups. *P*-values of ≤ 0.05 are considered statistically significant; the following asterisks are used to indicate the level of significance: $*P < 0.05$; $**P < 0.01$; $***P < 0.001$. *P*-values > 0.05 are considered not statistically significant (unmarked or specified as ns).

Data availability

Expanded View for this article is available online.

Acknowledgements

Author contributions

Athmane Teghanemt: Data curation; formal analysis; validation; investigation; writing – review and editing. **Kara Misel-Wuchter:** Formal analysis; investigation. **Jace Heath:** Formal analysis; investigation. **Andrew Thurman:** Data curation; software; validation; visualization; methodology. **Priyanjali Pulipati:** Formal analysis; investigation. **Garima Dixit:** Investigation; methodology. **Ramasatya Geesala:** Formal analysis; investigation. **David K Meyerholz:** Formal analysis; validation; investigation; methodology; writing – review and editing. **Thorsten Maretzky:** Supervision; writing – review and editing. **Alejandro Pezzulo:** Software; supervision; methodology; writing – review and editing. **Priya D Issuree:** Conceptualization; data curation; formal analysis; supervision; funding acquisition; validation; investigation; writing – original draft; project administration; writing – review and editing.

Disclosure and competing interests statement

The authors declare that they have no conflict of interest.

References

Bettelli E, Dastrange M, Oukka M (2005) Foxp3 interacts with nuclear factor of activated T cells and NF-kappa B to repress cytokine gene expression and effector functions of T helper cells. *Proc Natl Acad Sci USA* 102: 5138–5143

Boehm F, Martin M, Kesselring R, Schiechl G, Geissler EK, Schlitt HJ, Fichtner-Feigl S (2012) Deletion of Foxp3$^+$ regulatory T cells in genetically targeted mice supports development of intestinal inflammation. *BMC Gastroenterol* 12: 97

Bolger AM, Lohse M, Usadel B (2014) Trimmomatic: a flexible trimmer for Illumina sequence data. *Bioinformatics* 30: 2114–2120

Bruniquel D, Schwartz RH (2003) Selective, stable demethylation of the interleukin-2 gene enhances transcription by an active process. *Nat Immunol* 4: 235–240

Buenrostro JD, Giresi PG, Zaba LC, Chang HY, Greenleaf WJ (2013) Transposition of native chromatin for fast and sensitive epigenomic profiling of open chromatin, DNA-binding proteins and nucleosome position. *Nat Methods* 10: 1213–1218

Burchill MA, Yang J, Vogtenhuber C, Blazar BR, Farrar MA (2007) IL-2 receptor beta-dependent STAT5 activation is required for the development of Foxp3$^+$ regulatory T cells. *J Immunol* 178: 280–290

Chinen T, Kannan AK, Levine AG, Fan X, Klein U, Zheng Y, Gasteiger G, Feng Y, Fontenot JD, Rudensky AY (2016) An essential role for the IL-2 receptor in Treg cell function. *Nat Immunol* 17: 1322–1333

Darrigues J, Santamaria JC, Galindo-Albarran A, Robey EA, Joffre OP, van Meerwijk JPM, Romagnoli P (2021) Robust intrathymic development of regulatory T cells in young NOD mice is rapidly restrained by recirculating cells. *Eur J Immunol* 51: 580–593

Davidson TS, DiPaolo RJ, Andersson J, Shevach EM (2007) Cutting edge: IL-2 is essential for TGF-beta-mediated induction of Foxp3$^+$ T regulatory cells. *J Immunol* 178: 4022–4026

Eberl G, Littman DR (2004) Thymic origin of intestinal alphabeta T cells revealed by fate mapping of RORgammat$^+$ cells. *Science* 305: 248–251

Erben U, Loddenkemper C, Doerfel K, Spieckermann S, Haller D, Heimesaat MM, Zeitz M, Siegmund B, Kuhl AA (2014) A guide to histomorphological evaluation of intestinal inflammation in mouse models. *Int J Clin Exp Pathol* 7: 4557–4576

Fan MY, Low JS, Tanimine N, Finn KK, Priyadharshini B, Germana SK, Kaech SM, Turka LA (2018) Differential roles of IL-2 signaling in developing versus mature Tregs. *Cell Rep* 25: 1204–1213

Fantini MC, Becker C, Monteleone G, Pallone F, Galle PR, Neurath MF (2004) Cutting edge: TGF-beta induces a regulatory phenotype in CD4$^+$CD25$^-$ T cells through Foxp3 induction and down-regulation of Smad7. *J Immunol* 172: 5149–5153

Floess S, Freyer J, Siewert C, Baron U, Olek S, Polansky J, Schlawe K, Chang HD, Bopp T, Schmitt E *et al* (2007) Epigenetic control of the foxp3 locus in regulatory T cells. *PLoS Biol* 5: e38

Fontenot JD, Rudensky AY (2005) A well adapted regulatory contrivance: regulatory T cell development and the forkhead family transcription factor Foxp3. *Nat Immunol* 6: 331–337

Fontenot JD, Rasmussen JP, Gavin MA, Rudensky AY (2005) A function for interleukin 2 in Foxp3-expressing regulatory T cells. *Nat Immunol* 6: 1142–1151

Gilmour KC, Pine R, Reich NC (1995) Interleukin 2 activates STAT5 transcription factor (mammary gland factor) and specific gene expression in T lymphocytes. *Proc Natl Acad Sci USA* 92: 10772–10776

Harbour SN, Maynard CL, Zindl CL, Schoeb TR, Weaver CT (2015) Th17 cells give rise to Th1 cells that are required for the pathogenesis of colitis. *Proc Natl Acad Sci USA* 112: 7061–7066

Hemmers S, Schizas M, Azizi E, Dikiy S, Zhong Y, Feng Y, Altan-Bonnet G, Rudensky AY (2019) IL-2 production by self-reactive CD4 thymocytes scales regulatory T cell generation in the thymus. *J Exp Med* 216: 2466–2478

Issuree PD, Day K, Au C, Raviram R, Zappile P, Skok JA, Xue HH, Myers RM, Littman DR (2018) Stage-specific epigenetic regulation of CD4 expression by coordinated enhancer elements during T cell development. *Nat Commun* 9: 3594

Josefowicz SZ, Lu LF, Rudensky AY (2012) Regulatory T cells: mechanisms of differentiation and function. *Annu Rev Immunol* 30: 531–564

Kitagawa Y, Ohkura N, Kidani Y, Vandenbon A, Hirota K, Kawakami R, Yasuda K, Motooka D, Nakamura S, Kondo M *et al* (2017) Guidance of regulatory T

cell development by Satb1-dependent super-enhancer establishment. *Nat Immunol* 18: 173–183

Kuleshov MV, Jones MR, Rouillard AD, Fernandez NF, Duan Q, Wang Z, Koplev S, Jenkins SL, Jagodnik KM, Lachmann A *et al* (2016) Enrichr: a comprehensive gene set enrichment analysis web server 2016 update. *Nucleic Acids Res* 44: W90–W97

Lee YK, Turner H, Maynard CL, Oliver JR, Chen D, Elson CO, Weaver CT (2009) Late developmental plasticity in the T helper 17 lineage. *Immunity* 30: 92–107

Li MO, Rudensky AY (2016) T cell receptor signalling in the control of regulatory T cell differentiation and function. *Nat Rev Immunol* 16: 220–233

Lio CJ, Rao A (2019) TET enzymes and 5hmC in adaptive and innate immune systems. *Front Immunol* 10: 210

Marshall D, Sinclair C, Tung S, Seddon B (2014) Differential requirement for IL-2 and IL-15 during bifurcated development of thymic regulatory T cells. *J Immunol* 193: 5525–5533

McKarns SC, Schwartz RH, Kaminski NE (2004) Smad3 is essential for TGF-beta 1 to suppress IL-2 production and TCR-induced proliferation, but not IL-2-induced proliferation. *J Immunol* 172: 4275–4284

Meyerholz DK, Beck AP (2018) Principles and approaches for reproducible scoring of tissue stains in research. *Lab Invest* 98: 844–855

Miyara M, Gorochov G, Ehrenstein M, Musset L, Sakaguchi S, Amoura Z (2011) Human FoxP3⁺ regulatory T cells in systemic autoimmune diseases. *Autoimmun Rev* 10: 744–755

Moran AE, Holzapfel KL, Xing Y, Cunningham NR, Maltzman JS, Punt J, Hogquist KA (2011) T cell receptor signal strength in Treg and iNKT cell development demonstrated by a novel fluorescent reporter mouse. *J Exp Med* 208: 1279–1289

Moran-Crusio K, Reavie L, Shih A, Abdel-Wahab O, Ndiaye-Lobry D, Lobry C, Figueroa ME, Vasanthakumar A, Patel J, Zhao X *et al* (2011) Tet2 loss leads to increased hematopoietic stem cell self-renewal and myeloid transformation. *Cancer Cell* 20: 11–24

Mottet C, Uhlig HH, Powrie F (2003) Cutting edge: cure of colitis by CD4⁺CD25⁺ regulatory T cells. *J Immunol* 170: 3939–3943

Ohkura N, Hamaguchi M, Morikawa H, Sugimura K, Tanaka A, Ito Y, Osaki M, Tanaka Y, Yamashita R, Nakano N *et al* (2012) T cell receptor stimulation-induced epigenetic changes and Foxp3 expression are independent and complementary events required for Treg cell development. *Immunity* 37: 785–799

Owen DL, Farrar MA (2019) *In vitro* differentiation of thymic Treg cell progenitors to mature thymic Treg cells. *Bio Protoc* 9: e3335

Owen DL, Mahmud SA, Vang KB, Kelly RM, Blazar BR, Smith KA, Farrar MA (2018) Identification of cellular sources of IL-2 needed for regulatory T cell development and homeostasis. *J Immunol* 200: 3926–3933

Placek K, Hu G, Cui K, Zhang D, Ding Y, Lee JE, Jang Y, Wang C, Konkel JE, Song J *et al* (2017) MLL4 prepares the enhancer landscape for Foxp3 induction via chromatin looping. *Nat Immunol* 18: 1035–1045

Polansky JK, Kretschmer K, Freyer J, Floess S, Garbe A, Baron U, Olek S, Hamann A, von Boehmer H, Huehn J (2008) DNA methylation controls Foxp3 gene expression. *Eur J Immunol* 38: 1654–1663

Popmihajlov Z, Xu D, Morgan H, Milligan Z, Smith KA (2012) Conditional IL-2 gene deletion: consequences for T cell proliferation. *Front Immunol* 3: 102

Rubtsov YP, Rasmussen JP, Chi EY, Fontenot J, Castelli L, Ye X, Treuting P, Siewe L, Roers A, Henderson WR Jr *et al* (2008) Regulatory T cell-derived interleukin-10 limits inflammation at environmental interfaces. *Immunity* 28: 546–558

Sakaguchi S, Yamaguchi T, Nomura T, Ono M (2008) Regulatory T cells and immune tolerance. *Cell* 133: 775–787

Sakaguchi S, Mikami N, Wing JB, Tanaka A, Ichiyama K, Ohkura N (2020) Regulatory T cells and human disease. *Annu Rev Immunol* 38: 541–566

Sellars M, Huh JR, Day K, Issuree PD, Galan C, Gobeil S, Absher D, Green MR, Littman DR (2015) Regulation of DNA methylation dictates Cd4 expression during the development of helper and cytotoxic T cell lineages. *Nat Immunol* 16: 746–754

Shen L, Inoue A, He J, Liu Y, Lu F, Zhang Y (2014) Tet3 and DNA replication mediate demethylation of both the maternal and paternal genomes in mouse zygotes. *Cell Stem Cell* 15: 459–471

Tani-ichi S, Shimba A, Wagatsuma K, Miyachi H, Kitano S, Imai K, Hara T, Ikuta K (2013) Interleukin-7 receptor controls development and maturation of late stages of thymocyte subpopulations. *Proc Natl Acad Sci USA* 110: 612–617

Teghanemt A, Pulipati P, Misel-Wuchter K, Day K, Yorek MS, Yi R, Keen HL, Au C, Maretzky T, Gurung P *et al* (2022) CD4 expression in effector T cells depends on DNA demethylation over a developmentally established stimulus-responsive element. *Nat Commun* 13: 1477

Thiault N, Darrigues J, Adoue V, Gros M, Binet B, Perals C, Leobon B, Fazilleau N, Joffre OP, Robey EA *et al* (2015) Peripheral regulatory T lymphocytes recirculating to the thymus suppress the development of their precursors. *Nat Immunol* 16: 628–634

Toker A, Engelbert D, Garg G, Polansky JK, Floess S, Miyao T, Baron U, Duber S, Geffers R, Giehr P *et al* (2013) Active demethylation of the Foxp3 locus leads to the generation of stable regulatory T cells within the thymus. *J Immunol* 190: 3180–3188

Tsagaratou A, Aijo T, Lio CW, Yue X, Huang Y, Jacobsen SE, Lahdesmaki H, Rao A (2014) Dissecting the dynamic changes of 5-hydroxymethylcytosine in T-cell development and differentiation. *Proc Natl Acad Sci USA* 111: E3306–E3315

Tsagaratou A, Gonzalez-Avalos E, Rautio S, Scott-Browne JP, Togher S, Pastor WA, Rothenberg EV, Chavez L, Lahdesmaki H, Rao A (2017) TET proteins regulate the lineage specification and TCR-mediated expansion of iNKT cells. *Nat Immunol* 18: 45–53

Wang L, Ray A, Jiang X, Wang JY, Basu S, Liu X, Qian T, He R, Dittel BN, Chu Y (2015) T regulatory cells and B cells cooperate to form a regulatory loop that maintains gut homeostasis and suppresses dextran sulfate sodium-induced colitis. *Mucosal Immunol* 8: 1297–1312

Wu X, Zhang Y (2017) TET-mediated active DNA demethylation: mechanism, function and beyond. *Nat Rev Genet* 18: 517–534

Wu Y, Borde M, Heissmeyer V, Feuerer M, Lapan AD, Stroud JC, Bates DL, Guo L, Han A, Ziegler SF *et al* (2006) FOXP3 controls regulatory T cell function through cooperation with NFAT. *Cell* 126: 375–387

Yang R, Qu C, Zhou Y, Konkel JE, Shi S, Liu Y, Chen C, Liu S, Liu D, Chen Y *et al* (2015) Hydrogen sulfide promotes Tet1- and Tet2-mediated Foxp3 demethylation to drive regulatory T cell differentiation and maintain immune homeostasis. *Immunity* 43: 251–263

Yao Z, Kanno Y, Kerenyi M, Stephens G, Durant L, Watford WT, Laurence A, Robinson GW, Shevach EM, Moriggl R *et al* (2007) Nonredundant roles for Stat5a/b in directly regulating Foxp3. *Blood* 109: 4368–4375

Yue X, Trifari S, Aijo T, Tsagaratou A, Pastor WA, Zepeda-Martinez JA, Lio CW, Li X, Huang Y, Vijayanand P *et al* (2016) Control of Foxp3 stability through modulation of TET activity. *J Exp Med* 213: 377–397

Yue X, Lio CJ, Samaniego-Castruita D, Li X, Rao A (2019) Loss of TET2 and TET3 in regulatory T cells unleashes effector function. *Nat Commun* 10: 2011

Zheng SG, Wang J, Wang P, Gray JD, Horwitz DA (2007) IL-2 is essential for TGF-beta to convert naive CD4$^+$CD25$^-$ cells to CD25$^+$Foxp3$^+$ regulatory T cells and for expansion of these cells. *J Immunol* 178: 2018–2027

Zheng Y, Josefowicz S, Chaudhry A, Peng XP, Forbush K, Rudensky AY (2010) Role of conserved non-coding DNA elements in the Foxp3 gene in regulatory T-cell fate. *Nature* 463: 808–812